metals

MDPI

Article

First-Principles Study on the Effect of Si Atoms on the Stability and Bonding Properties of Fe/Zn Interface

Degao Qiao [1,2], Peng Peng [1,*], Xingchang Tang [3,*], Junqiang Ren [3], Xuefeng Lu [3] and Jie Sheng [3]

[1] School of Materials and Energy, Lanzhou University, Lanzhou 730050, China; qiaodegao@jiugang.com
[2] Carbon Steel Sheet Factory, Jiuquan Iron and Steel (Group) Co., Ltd., Jiayuguan 735100, China
[3] State Key Laboratory of Advanced Processing and Recycling of Non-Ferrous Metals, School of Materials Science and Engineering, Lanzhou University of Technology, Lanzhou 730050, China; renjq@lut.edu.cn (J.R.); lxfeng@lut.edu.cn (X.L.); shengjie@lut.edu.cn (J.S.)
* Correspondence: pengp@lzu.edu.cn (P.P.); tangxc@lut.edu.cn (X.T.); Tel.: +86-0931-2976688 (X.T.)

Abstract

The stability of the Fe/Zn interface during the hot-dip galvanizing process critically influences the coating's quality and service performance. In this investigation, the impact of silicon atom positioning on the stability, bonding strength, and electronic structure of the Fe/Zn interface was systematically examined through first-principles calculations grounded in density functional theory, employing the CASTEP software and the GGA-PBE functional. By constructing the FeSi and ZnSi disordered solid solution models, low-energy stable configurations were selected, and 24 ZnSi/FeSi interface models (misfit < 5%) were further established. The interfacial adhesion work, interfacial energy, and electronic structure parameters were systematically calculated. The findings indicate that the position of Si atoms significantly affects interface stability, with Si atoms located on the Zn side exerting a more pronounced influence than those on the Fe side. The interfacial stability is optimal when the Si on the Fe side is far away from the interface and the Si on the Zn side is located at the interface. Notably, the S11Z32 model exhibited the highest adhesion work (4.763 J/m^2) and the lowest interface energy (0.022 J/m^2). This study elucidates the regulatory role of Si atoms in stabilizing the Fe/Zn interface and provides a theoretical foundation for optimizing the hot-dip galvanizing process and guiding the design of novel materials.

Keywords: first-principles; Fe/Zn interface; interface stability; interfacial energy

1. Introduction

In the discipline of materials science and engineering, the enhancement of material properties is critical for the advancement of high-performance materials. Recently, as steel materials have evolved towards greater performance and multifunctionality, interface engineering has emerged as a pivotal approach to augment material performance. Specifically, the Fe/Zn interface, which is fundamental in the hot-dip galvanizing process, significantly influences both the coating quality and the overall service performance of the materials [1]. The incorporation of trace elements is instrumental in modulating the microstructure and macroscopic characteristics of materials. Among these, silicon (Si) is particularly significant in material design and regulation owing to its distinctive physical and chemical attributes [2].

Hot-dip galvanizing technology represents one of the most cost-effective and efficient methods for mitigating the corrosion of steel. The fundamental mechanism involves the wetting, diffusion, and interfacial reactions of zinc on the iron substrate. Research indicates

Check for updates

Academic Editor: Changming Fang

Received: 17 October 2025
Revised: 2 December 2025
Accepted: 30 December 2025
Published: 1 January 2026

Copyright: © 2026 by the authors. Licensee MDPI, Basel, Switzerland. This article is an open access article distributed under the terms and conditions of the Creative Commons Attribution (CC BY) license.

that the formation and stability of the Fe/Zn interface are influenced by multiple factors, including temperature, pressure, crystallographic orientation of the interface, and the presence of alloying elements [3]. Insufficient stability at the Fe/Zn interface can lead to the decomposition or reaction of intermetallic compounds, which subsequently diminishes the adhesion strength between the coating and the substrate. This degradation may result in coating delamination, thereby compromising the protective performance of the galvanized layer. Previous investigations have demonstrated that when the steel substrate contains silicon in the range of 0.06 to 0.10 wt%, the so-called "Sandelin effect" is induced at the interface, characterized by an anomalous increase in the thickness of the zinc coating [4,5]. Experimental studies have suggested that this phenomenon is closely associated with the formation of silicon-rich phases, such as FeSi and Fe_2SiO_3, at the interface. The underlying mechanism involves a eutectic reaction within the Fe-Zn-Si ternary system, wherein the liquid metal decomposes into a mixed phase comprising ζ, η, and FeSi. This reaction facilitates direct contact between the liquid zinc and the steel substrate, thereby accelerating the rapid formation of the ζ phase and resulting in a significant increase in coating thickness [6]. In silicon steel, silicon exists in solid solution, and its diffusion coefficient varies with concentration. An increase in silicon content reduces the activation energy for carbon diffusion, thereby enhancing the carbon diffusion coefficient and promoting decarburization. At a silicon concentration of 3.5 wt%, silicon diffuses toward the near-surface region and forms a continuous banded SiO_2 layer in conjunction with residual oxygen. Conversely, at a silicon content of 1.5 wt%, the diffusion coefficient of silicon is lower, leading to oxidation of residual oxygen with silicon within the matrix, resulting in a highly dispersed SiO_2 phase that does not form a banded structure [7]. The thickness of the coating in hot-dip Zn-Al-Mg-Si alloy-coated steel with silicon addition is markedly reduced, accompanied by the formation of a stable Fe_2Al_3Si inhibition layer at the interface. Additionally, a needle-like Mg_2Si phase develops on the coating surface. The incorporation of silicon suppresses the interdiffusion between iron and coating elements, thereby enhancing the coating's adhesion. Furthermore, an increase in silicon content correlates with improved corrosion resistance of the coating [8]. In recent years, advancements in computational materials science have established first-principles calculation methods as powerful tools for investigating metal interfaces. Utilizing density functional theory and related computational techniques, researchers can simulate interface structures at the atomic scale, compute stability parameters such as interface energy, and analyze the behavior of specific elements at the interface. These computational approaches not only offer detailed microstructural insights but also elucidate the mechanisms underlying experimental observations, thereby providing theoretical guidance for material design and process optimization. For instance, Sun et al. [9] demonstrated that the diffusion of silicon atoms within γ-Ni and γ′-Ni3Fe supercell systems results in an increased diffusion energy barrier, while the formation enthalpy and total energy of oxygen-doped silicon are minimized. In the Fe/Cu interface system examined by Wang et al. [3], silicon exhibits a pronounced tendency to segregate within the iron matrix, which diminishes the interfacial covalent interactions via charge transfer. Furthermore, Wang et al. [10] explored the influence of alloying elements X (Cr, Mn, Mo, Ni, and Si) in 316L stainless steel on the stability of the TiC(001)/γ-Fe(001) interface. Their findings indicate that the incorporation of silicon facilitates the formation of specific chemical bonds, thereby promoting the heterogeneous nucleation of iron on TiC, enhancing the nucleation potential of TiC, and strengthening the interfacial bonding in TiC/316L stainless steel composites.

Current research on the Fe/Zn interface predominantly emphasizes experimental observations and macroscopic performance characterization, with relatively limited theoretical investigations at the atomic scale. Notably, there is a lack of systematic theoretical

analysis regarding the effect of Si atoms on the stability of the Fe/Zn interface. In this study, first-principles calculations are employed to evaluate critical parameters—including interface adhesion work, interface energy—by constructing Fe/Zn interface models with Si atoms positioned at various sites. This research aims to elucidate the mechanisms by which Si atoms influence the stability of the Fe/Zn interface, thereby providing a theoretical foundation for optimizing the hot-dip galvanizing process and guiding the design of novel materials. Furthermore, the findings are expected to contribute positively to the application and advancement of steel materials.

2. Computational Details

The calculation uses the CASTEP (Cambridge Serial Total Energy Package) software package (MS 2023V) [11] based on the density functional theory plane wave pseudopotential method, and the Perdew–Burke–Eruzerhof (PBE) algorithm of the generalized gradient approximation (generalized gradient approximation, GGA) is used to describe the exchange correlation energy [12]. The interaction between the nucleus and the electron is described by the ultra-soft pseudopotential. The Broyden–Fletcher–Goldfarb–Shanno (BFGS) method was employed to relax the positions of all atoms in order to obtain the minimum structural energy. The convergence criteria for the geometric optimization were as follows: the total energy convergence threshold was set at 5.0×10^{-6} eV/atom, the force on each atom was required to be less than 0.01 eV/Å, the stress deviation was limited to less than 0.02 GPa, the maximum tolerance for atomic displacement was less than 5.0×10^{-4} Å, and the self-consistent field (SCF) convergence energy was set at 1.0×10^{-6} eV/atom. Furthermore, during the modeling of surfaces and interfaces, periodic boundary conditions can cause interactions between neighboring elements, which may compromise the accuracy of the calculations. To effectively separate adjacent phase structures and reduce the impact of surface interactions, a vacuum layer of 15 Å was introduced into the corresponding surface and interface models [13–16].

In this study, we conducted a convergence test for the plane wave truncation energy (Ecutoff) and the k-point to determine suitable computational parameters. The methodology employed is as follows: initially, the k-point is established at $10 \times 10 \times 10$, and the Ecutoff value is incrementally increased until the system's single-point energy converges. Subsequently, with the Ecutoff value held constant, the k-point is progressively increased, allowing for the selection of appropriate parameters based on the convergence of the single-point energy. The convergence test results are shown in the Supporting Materials. Based on the convergence test results and computing resources, the truncation energy was set to 380 eV, and the k point was set to $8 \times 8 \times 8$.

3. Results and Discussion

3.1. Bulk Calculations

To evaluate the reliability of the computational parameters and methodologies, as well as the validity of the initial crystal structure, the lattice constants of bcc-Fe and hcp-Zn were calculated using various exchange-correlation functionals, including LDA-CAPZ, GGA-PW91, and GGA-PBE. The valence electrons of the atoms are calculated as Fe-$3d^6 4s^2$, Zn-$3d^{10} 4s^2$, and Si-$3s^2 3p^2$, and the results are shown in the Supporting Materials. Additionally, theoretical and experimental lattice constant data from the literature were incorporated for comparative analysis. Notably, the lattice constants derived from structural optimization employing the GGA-PBE functional exhibit closer agreement with both theoretical predictions and experimental measurements reported in the literature. This concordance suggests that the parameter settings and data utilized in the present study are appropriate and reliable.

In calculating the phonon spectrum, whether the frequencies are real or imaginary is crucial for determining the stability of a crystal structure within the harmonic approximation. If the phonon spectrum shows no imaginary frequencies across all wave vectors, the crystal is dynamically stable under this approximation. This means the lattice strongly resists small deformations, and there is no tendency for spontaneous structural phase transitions. At finite temperatures, the phonon contribution to the free energy is real, allowing normal calculation of thermodynamic properties. Conversely, the presence of imaginary frequencies indicates structural instability. When a molecule is dynamically unstable but mechanically stable, it can exist in a metastable state [17,18]. To demonstrate the dynamic stability of body-centered cubic iron (bcc-Fe) and hexagonal close-packed zinc (hcp-Zn), phonon dispersion curves were computed using the linear response method. As illustrated in Figure 1, the phonon spectra for both bcc-Fe and hcp-Zn exhibited no imaginary frequencies, indicating that these phases are dynamically stable.

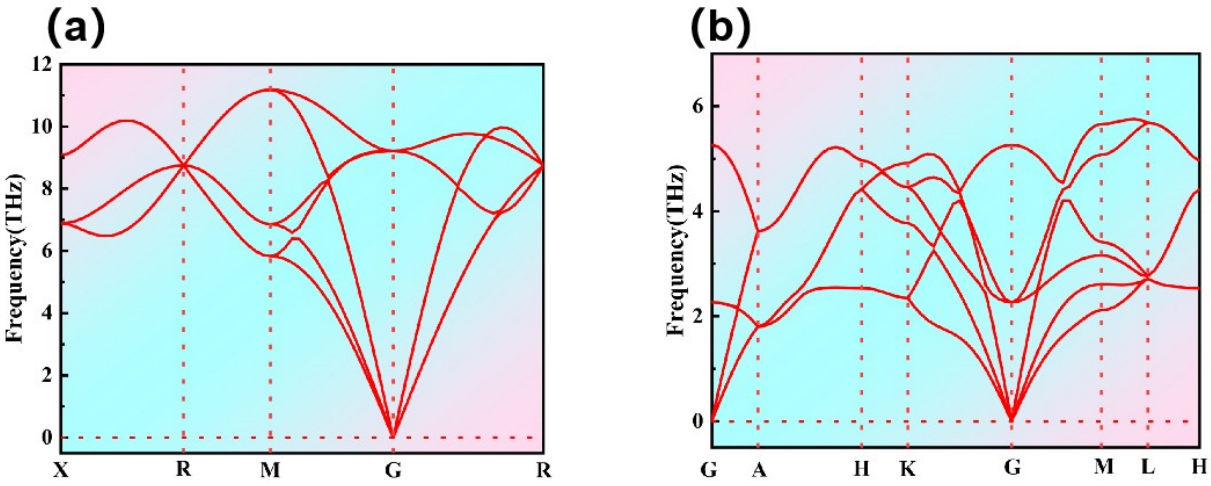


Figure 1. The phonon dispersion of bcc-Fe and hcp-Zn: (**a**) the phonon spectrum of bcc-Fe has no imaginary frequency; (**b**) the phonon spectrum of hcp-Zn has no imaginary frequency.

To identify the appropriate interface orientation type, the interface model was assessed based on surface energy and interface mismatch, as established in prior studies [19–21]. This investigation focused on low-index surfaces, specifically the Fe(110) and Zn(110) planes. For Zn, the low-index surfaces considered included the (111), (100), and (110) crystallographic planes; however, the surface energy differences among these three planes were minimal, suggesting comparable stability across these surfaces. In contrast, the low-index surfaces of Fe encompassed the (110), (100), (210), (111), (121), and (323) planes. Notably, the Fe(110) surface exhibited the lowest surface energy, indicating its relative stability and suitability for constructing the interface model [22]. Increasing the number of atomic layers in the surface structure enhances the accuracy of representing the internal characteristics of the material block and more faithfully reflects the actual interface system. As illustrated in Figure 2, for the Zn(110) surface, variations in the interlayer spacing beyond eight atomic layers were negligible; therefore, an eight-layer Zn slab was employed in subsequent simulations. Conversely, a five-layer atomic structure sufficed for the Fe(110) surface. In Figure 2b,e, S1 and S2 denote two distinct terminations of the Fe(110) surface, while Z1, Z2, and Z3 represent three different terminations of the Zn(110) surface.

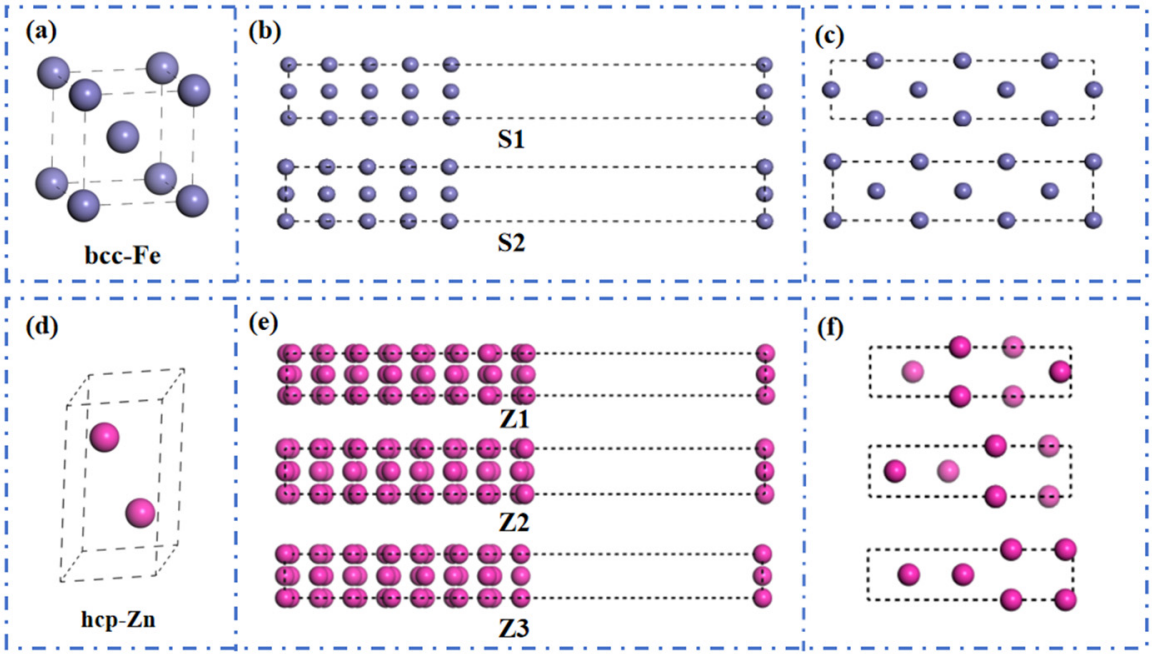


Figure 2. Initial volume and surface models: (**a**) Fe bulk phase model; (**b**) front view of S1 and S2 terminal models on Fe(110) surface; (**c**) top view of S1 and S2 terminal models on Fe(110) surface; (**d**) Zn bulk phase model; (**e**) front view of Z1, Z2 and Z3 terminal models on Zn(110) surface; (**f**) top view of Z1, Z2 and Z3 terminal models on Zn(110) surface.

3.2. Disordered Solid Solution Structure of ZnSi Coating Alloy

In the calculation, the structure of the disordered alloy solid solution was established using the Perl script [23]. Based on the substitution atoms and the Shuffle function in the CASTEP module, the Perl script randomly replaces the matrix elements in a certain proportion to form a disordered solid solution. The original cell of the body-centered cubic Fe was cut out of the Fe(110) surface structure and expanded as the matrix of the disordered alloy solid solution. The number of atoms in the surface model was 30, a was 11.6565 Å, b was 2.7474 Å, and c was 22.7710 Å. The Zn(110) surface structure was cut out from the original hexagonal Zn cell and expanded. The number of atoms in the surface model was 32, a was 10.9173 Å, b was 2.6649 Å, and c was 29.9887 Å. Figure 3 assigns numerical labels to the Fe(110) surface structures for concise description. S11 denotes Si within the substrate, while S12 indicates Si on the substrate surface. The structure labeled 0 represents a clean interface, whereas the 1–15 numbered structures represent disordered solid solution configurations of these interfaces. Other model structures are detailed in the Supplementary Materials.

In accordance with the principle of minimum energy, this study performed relaxation on all surface models and calculated the energies of each random model of disordered solid solutions using the single-point energy module. The results are shown in Figure 4. The disordered solid solution structures with the lowest energies at the S11, S12, S21, S22, T11, T12, T21, T22, T31, and T32 terminals are ranked as 14, 9, 11, 10, 4, 6, 4, 6, 7, and 7, respectively. Therefore, these structures with the lowest energy numbers are identified as low-energy stable configurations.

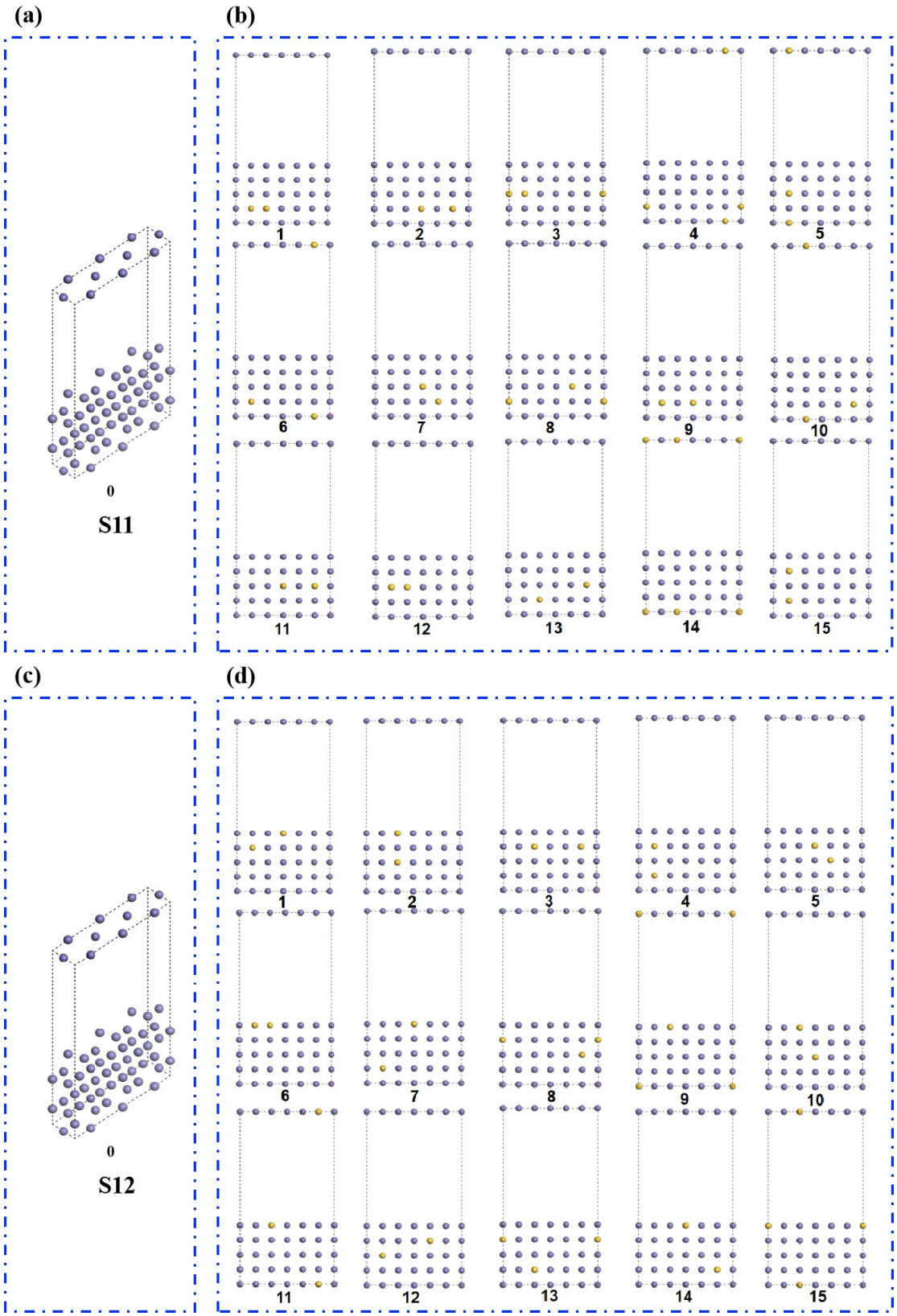


Figure 3. Model diagram of the disordered solid solution structure between the FeSi matrix and ZnSi coating: (**a**) S11 terminal; (**b**)15 disordered solid solution structures of S11 terminal; (**c**) S12 terminal; (**d**) 15 disordered solid solution structures of S12 terminal. The Fe atoms are colored blue, and the Si atoms are colored yellow.

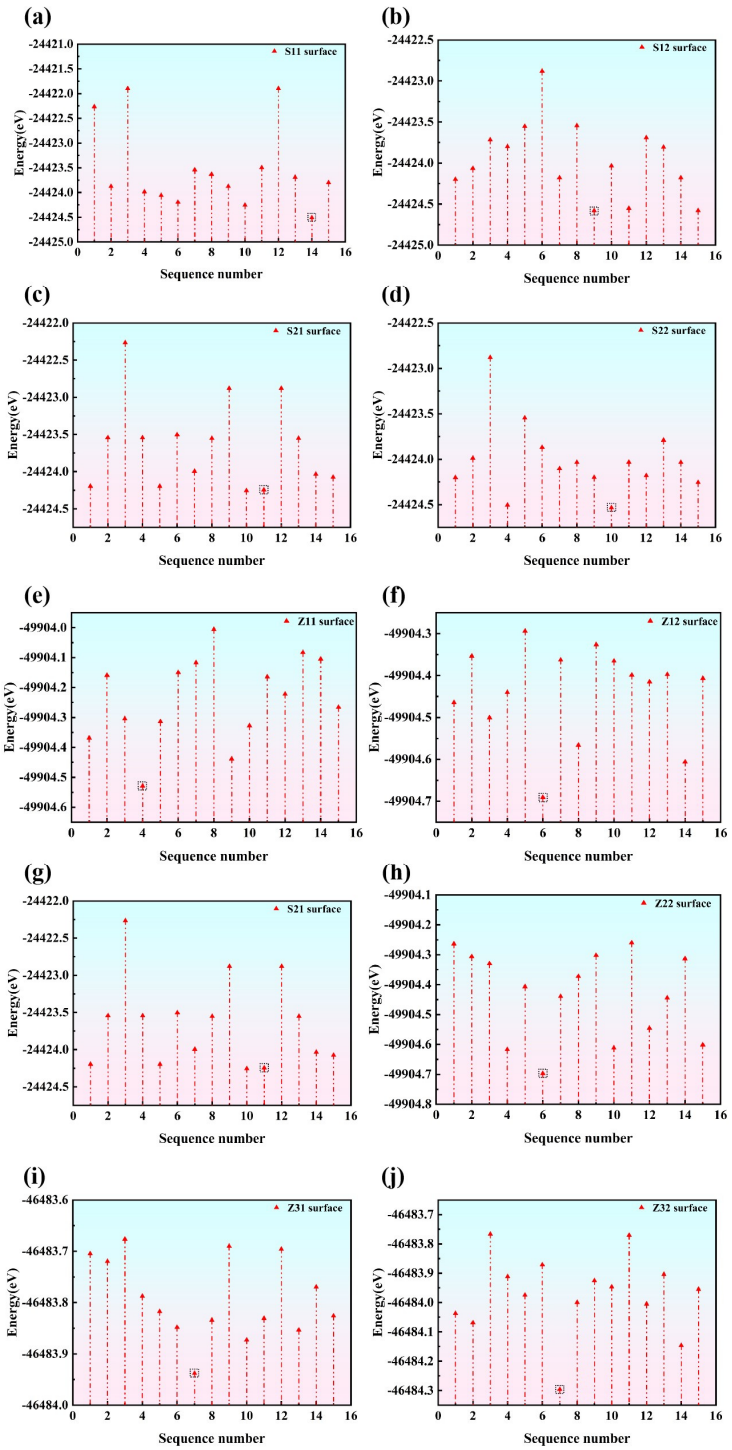


Figure 4. Energy of disordered solid solution structure system for FeSi matrix and ZnSi coating. (**a**) The terminal with the lowest energy in S11 disordered solid solution is numbered 14; (**b**) The terminal with the lowest energy in S12 disordered solid solution is numbered 9; (**c**) The terminal with the lowest energy in S21 disordered solid solution is numbered 11; (**d**) The terminal with the lowest energy in S22 disordered solid solution is numbered 10; (**e**) The terminal with the lowest energy in Z11 disordered solid solution is numbered 4; (**f**) The terminal with the lowest energy in Z12 disordered solid solution is numbered 6; (**g**) The terminal with the lowest energy in Z21 disordered solid solution is numbered 4; (**h**) The terminal with the lowest energy in Z22 disordered solid solution is numbered 6; (**i**) The terminal with the lowest energy in Z31 disordered solid solution is numbered 7; (**j**) The terminal with the lowest energy in Z32 disordered solid solution is numbered 7. The dotted box represents the point with the lowest energy.

3.3. Interfacial Structure

A disordered solid solution model comprising an FeSi matrix and a ZnSi coating was employed to represent the splicing interface. To determine the optimal orientation relationship at the interface, an extensive investigation of potential crystallographic directions was conducted, with particular attention to the magnitude of interface mismatch. Ultimately, the Zn(110)/Fe(110) interface model was selected for this study. Given that mismatch stress could not be sufficiently alleviated through cell expansion alone, the surface model was reconstructed by redefining the lattice parameters to minimize the mismatch. This mismatch is quantified by the mismatch degree μ, which is defined according to the formula presented in reference [24]:

$$\mu = 1 - \frac{2\Omega}{A_1 + A_2} \quad (1)$$

The formula indicates that the overlap area of the Ω interface is 31.54 Å^2, with A1 and A2 representing the surface areas of the two constituent phases. After lattice reconstruction, the u and v dimensions of the FeSi (110) surface structure are 11.6565 Å and 2.7474 Å, respectively, while those of the ZnSi (110) surface structure are 10.9173 Å and 2.6649 Å. The values of A1 and A2 are 32.0258 Å^2 and 29.0935 Å^2, respectively. When the u-v angle is 90°, the interfacial mismatch between ZnSi (110) and FeSi (110) is 3.22%, below 5%. Thus, the interfacial model constructed in this study represents a valid structure. Calculations show a lattice mismatch of 2.03% in the a direction and 1.01% in the b direction.

The stacking configurations within the interface model exhibit varying degrees of energetic stability. Different stacking arrangements at the interface induce modifications in the electronic structure, manifesting as variations in charge density, density of states, and bond population metrics. Consequently, accurately predicting and comprehending the bonding characteristics at the interface is of critical importance. Figure 5 presents detailed representations of the interface structures. Specifically, the distinct terminations of FeSi and ZnSi are combined to generate a total of 24 interface models. The interface region comprises the upper two atomic layers of Fe and the lower three atomic layers of Zn. Following an optimization of the interfacial spacing, the separation distance was fixed at 2.2 Å. Additionally, a vacuum layer of 15 Å thickness was introduced at both ends of the model to prevent interactions between the surface atoms on the upper and lower boundaries. The notation SijZkl represents the surface model where S denotes Fe and Z denotes Zn. The terminal types are defined as i (Fe terminal type) and k (Zn terminal type), with j (Fe-side Si position) and l (Zn-side Si position) indicating 1 (Si away from interface) or 2 (Si at interface). For example, S11Z11 indicates a combination of Fe terminal 1 and Zn terminal 1, where Si on the Fe terminal is away from the interface, while Si on the Zn terminal remains at the interface. Similarly, S21Z32 describes a combination of Fe terminal 2 and Zn terminal 3, where Si on the Fe terminal is away from the interface, while Si on the Zn terminal exists at the interface.

3.4. Adhesion Work and Interfacial Energy

The work of adhesion (Wad) serves as a quantitative measure of the interfacial bonding strength between two materials. It denotes the reversible energy necessary to separate the interface from a bonded state into two distinct free surfaces, excluding contributions from plastic deformation and diffusion processes. A higher value of the work of adhesion indicates a stronger atomic interaction at the interface, reflecting a closer atomic arrangement

and enhanced interfacial stability [25]. The calculation of Wad can be conducted using the following equation [26,27]:

$$W_{ad} = \frac{E_{ZnSi}^{slab} + E_{FeSi}^{slab} - E_{FeSi/ZnSi}^{interface}}{A} \quad (2)$$

where E_{ZnSi}^{slab} and E_{FeSi}^{slab} represent energies of ZnSi(110) and FeSi(110) surface energy, and A and $E_{FeSi/ZnSi}^{interface}$ are the area and total energy of the interface, respectively.

The interfacial energy is the increment of the free energy of the unit interfacial system. The higher the interfacial energy, the more energy is required to form the interface, and the less stable the interface. Therefore, the smaller the interfacial energy, the more stable the interface [28]. The calculation formula (3) and (4) is as follows [29,30]:

$$\gamma_{MeSi} = \frac{1}{2A}\left[\gamma_{slab} - N_{Me}\gamma_{Me}^{bulk} - N_{Si}\gamma_{Si}^{bulk}\right] \quad (3)$$

The formula γ_{MeAl} represents the surface energy of MeSi (Me = Fe, Zn) surface, while γ_{slab} denotes the total energy of the MeAl (Me = Fe, Zn) surface model. N_{Me} and N_{Si}, respectively, indicate the quantities of Me (Me = Fe, Zn) atoms and Si atoms in the MeSi (Me = Fe, Zn) surface model.

$$\gamma_{int} = \gamma_{surf}^{FeSi} + \gamma_{surf}^{ZnSi} - W_{ad} \quad (4)$$

In the above formula, γ_{surf}^{FeSi} and γ_{surf}^{ZnSi} represent the surface energy of the FeSi surface model and the ZnSi surface model, respectively. According to the above relationship, the interfacial energy of the interface is obtained. The post-relaxation adhesion work and interfacial energy are shown in Table 1.

Table 1. Adhesion work (Wad) and interfacial energy (γint) of FeSi/ZnSi after full relaxation.

Connection Mode	Adhesion Work W_{ad} (J/m^2)	Interfacial Energy γ_{int} (J/m^2)
S11Z11	3.818	0.714
S11Z12	4.056	0.431
S11Z21	3.798	0.741
S11Z22	4.327	0.158
S11Z31	4.727	0.063
S11Z32	4.763	0.022
S21Z11	3.760	0.535
S21Z12	4.307	0.056
S21Z21	3.662	0.641
S21Z22	3.926	0.323
S21Z31	4.444	0.110
S21Z32	4.705	0.050
S12Z11	3.668	0.678
S12Z12	3.909	0.392
S12Z21	3.495	0.859
S12Z22	4.090	0.210
S12Z31	4.546	0.058
S12Z32	4.631	0.025
S22Z11	3.910	0.418
S22Z12	4.151	0.133
S22Z21	3.356	0.980
S22Z22	3.364	0.917
S22Z31	4.149	0.438
S22Z32	4.461	0.027



Figure 5. *Cont.*

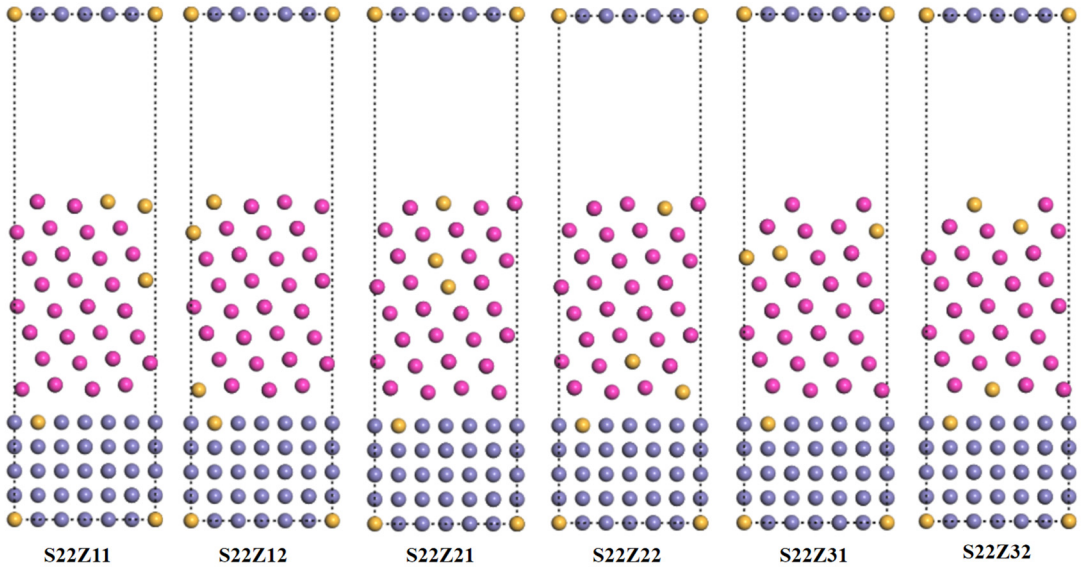


Figure 5. Twenty-four different ZnSi (110)/FeSi (110) interface structures. The Fe atoms are colored blue, Zn atoms are colored purple and the Si atoms are colored yellow.

Based on the above data analysis, Figure 6 shows the relationship between different interface models and interface energy and adhesion work. As depicted in Figure 6, there exists a pronounced negative correlation between adhesion work and interface energy; specifically, higher adhesion work corresponds to lower interface energy, which aligns with theoretical expectations. Notably, the adhesion work and interface energy vary considerably across different lap joint configurations, underscoring the significant influence of terminal type and Si position on interface stability. Among the configurations examined, the lap joint designated S11Z32 exhibits the highest adhesion work (4.763 J/m^2) and the lowest interface energy (0.022 J/m^2).

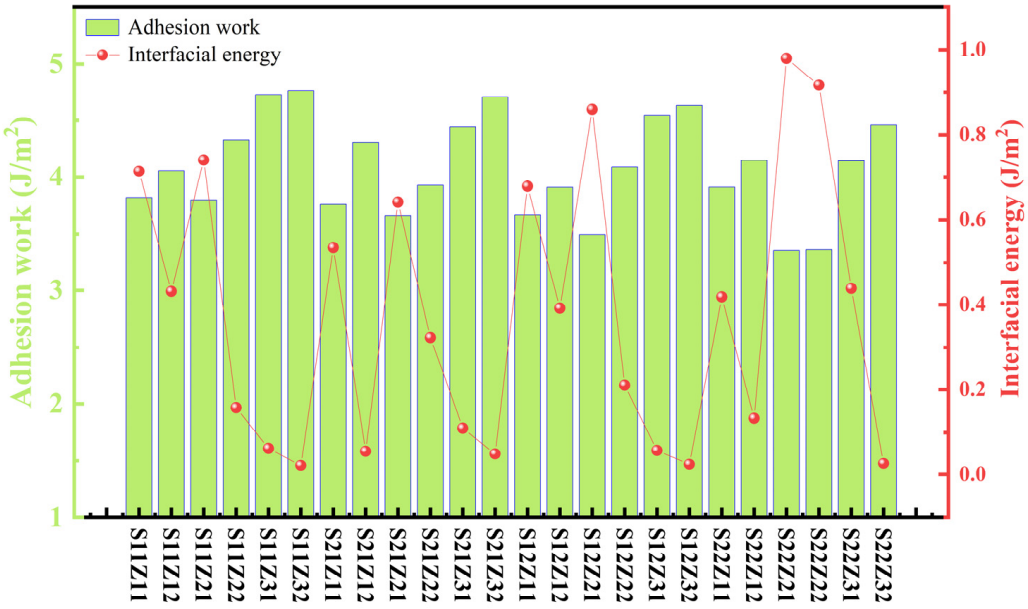


Figure 6. The relationship between different interface models and interface energy and adhesion work. The S11Z32 bonding mode has the highest adhesion work (4.763 J/m^2) and the lowest interfacial energy (0.022 J/m^2).

Figure 7 shows the effects of different interface terminals and silicon atom positions on the interfacial energy and adhesion work. Figure 7a,b further reveal that the differences in adhesion work and interface energy between Fe terminal types 1 and 2 are minimal. The average adhesion work for Fe terminal type 1 is marginally greater than that of type 2, while the average interface energy for type 1 is slightly lower, suggesting a modestly favorable effect of Fe terminal type 1 on interface stability. Overall, the influence of Fe terminal type on interface stability appears to be relatively minor. Figure 7c,d demonstrate that the type of Zn terminal exerts a significant influence on both the adhesion work and the interface energy. Variations in the Zn terminal type result in notable changes in adhesion work as well as in the average interface energy. Specifically, Zn terminal type 3 exhibits the highest average adhesion work and the lowest average interface energy, suggesting that this terminal configuration most effectively enhances interface stability. Furthermore, as illustrated in Figure 7e–h, the position of Si on the Fe side also impacts interface properties. When Si is positioned away from the interface (position 1), the adhesion work is marginally higher compared to when Si is located directly at the interface (position 2). Correspondingly, the interface energy is slightly lower at position 1 than at position 2, indicating that Si situated away from the interface on the Fe side contributes to improved interface stability. Conversely, for Si located on the Zn side, positioning at the interface (position 2) results in a markedly higher adhesion work and a significant reduction in interface energy relative to Si positioned away from the interface (position 1). This finding implies that Si presence at the interface on the Zn side enhances the stability of the interface.

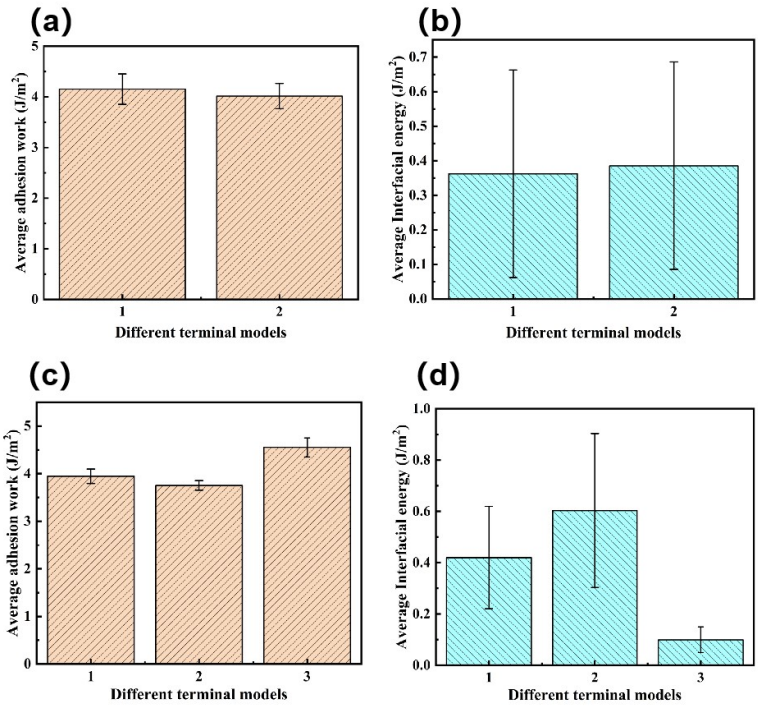


Figure 7. *Cont.*

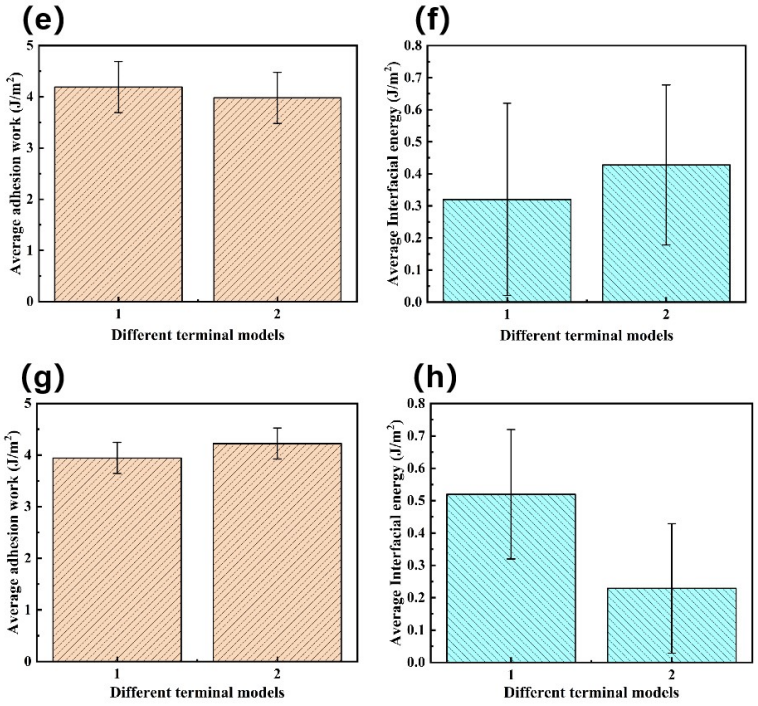


Figure 7. Effect of different interface terminals and Si atom positions on interface energy and adhesion work: (**a**) The difference in adhesion work between iron terminal type 1 and type 2 is small, and the average adhesion work of iron terminal type 1 is slightly higher than that of type 2. (**b**) The difference in interfacial energy between iron terminal types 1 and 2 is minimal, and the average interfacial energy of iron terminal type 1 is slightly lower than that of type 2. (**c**) Zn terminal 3 has the highest average adhesion power. (**d**) Zn terminal 3 has the lowest average interfacial energy. (**e**) When the Si is far from the interface (position 1), its adhesion work is slightly higher than that at the interface directly (position 2). (**f**) The interface energy of position 1 is slightly lower than that of position 2, indicating that Si on the Fe side away from the interface contributes to the improvement of interface stability. (**g**) When Si is located on the Zn side, the adhesion work at the interface position (position 2) is significantly higher. (**h**) When Si is located on the Zn side, the interface can be significantly reduced at a position away from the interface (position 1).

Analysis of the heat maps presented in Figure 8a–d reveals that the interface configuration combining Fe terminal type 1 with Zn terminal type 3 (denoted as S1Z3) exhibits the highest adhesion work alongside the lowest interface energy, indicating its superior contribution to enhancing interface stability. Specifically, the arrangement wherein the Si atom on the Fe side is positioned away from the interface, while the Si atom on the Zn side is located directly at the interface, demonstrates the most favorable combination for improving interface stability. Overall, the spatial positioning of Si atoms significantly influences the stability of the FeSi/ZnSi interface, with the effect of Si placement at the Zn terminal being more pronounced than that at the Fe terminal. Irrespective of the Si position at the Fe terminal, configurations with Si situated at the Zn terminal interface consistently show greater stability compared to those with Si positioned away from the interface. Furthermore, the stability is maximized when the Zn-terminal Si resides at the interface and the Fe-terminal Si is positioned distally from the interface. Consequently, the optimal structural configuration is characterized by Fe terminal type 1 Si located away from the interface, combined with Zn-terminal type 3 Si situated at the interface. Among the 24 interface models examined, the S11Z32 configuration of the FeSi/ZnSi interface is identified as the most thermodynamically stable.

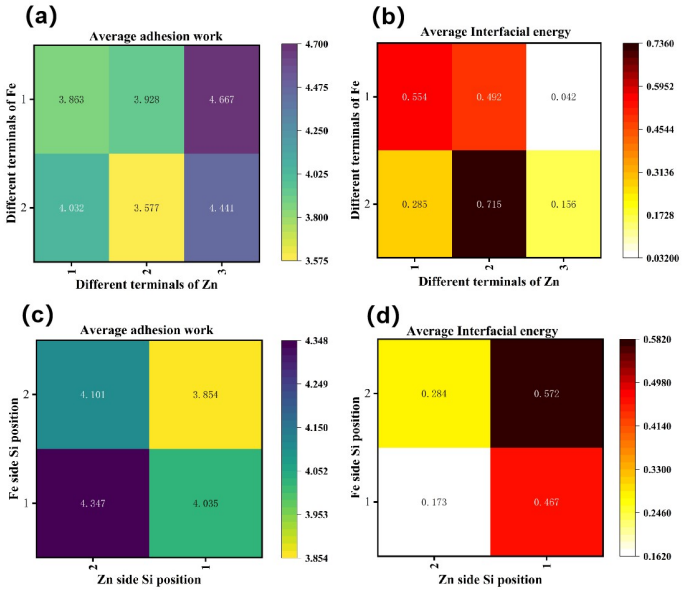


Figure 8. Relationship between interface energy and adhesion work of Si atoms at different interface terminals: (**a**–**d**) The interface configuration combining Fe end-type 1 and Zn end-type 3 (marked as S1Z3) showed the highest adhesion work and the lowest interfacial energy, indicating that it has a better contribution to enhance the interfacial stability.

4. Conclusions

This study examines the effect of silicon atom positioning on the interfacial bonding properties between iron and zinc using first-principles calculations. The investigation encompasses assessments of interface stability, bonding strength, and electronic structure. It is important to emphasize that, as foundational research, this work builds upon prevailing findings in the literature concerning iron-based alloys. Through a systematic analysis, the following principal conclusions have been derived: A total of 24 distinct interface models were evaluated. Each type of interface is established for different terminals or the location of Si is different. The effect of Si position on the stability of the FeSi/ZnSi interface is significant, and the effect of Si position at the Zn end is stronger than that of the Si position at the Fe end. The combination of the Fe-side Si away from the interface and the Zn-side Si at the interface has the highest adhesion work and the lowest interface energy, which is the most favorable Si position combination to improve the interface stability.

Supplementary Materials: The following supporting information can be downloaded at: https://www.mdpi.com/article/10.3390/met16010056/s1. References [31–33] are cited in the supplementary materials.

Author Contributions: Conceptualization, P.P. and X.T.; methodology, J.R. and D.Q.; software, P.P. and J.R.; validation, J.S.; formal analysis, J.S.; investigation, X.L. and D.Q.; data curation, J.S. and X.L.; writing—original draft preparation, D.Q.; writing—review and editing, J.R.; visualization, X.L.; supervision, P.P. and X.T.; project administration, X.T.; funding acquisition, X.T. All authors have read and agreed to the published version of the manuscript.

Funding: This project is financially supported by the Jiayuguan City major science and technology special fund (23-01), Jiayuguan City key research and development plan (24-11).

Data Availability Statement: The original contributions presented in this study are included in the article/Supplementary Material. Further inquiries can be directed to the corresponding authors.

Conflicts of Interest: Degao Qiao was employed by Carbon Steel Sheet Factory, Jiuquan Iron and Steel (Group) Co., Ltd. The remaining authors declare that the research was conducted in the absence of any commercial or financial relationships that could be construed as a potential conflict of interest.

References

1. Fukazawa, T.; Harashima, Y.; Miyake, T. First-principles study on the stability of (R, Zr)(Fe, Co, Ti) 12 against 2-17 and unary phases (R = Y, Nd, Sm). *Phys. Rev. Mater.* **2022**, *6*, 054404. [CrossRef]
2. Jiao, X.; Fu, W.; Shi, Z.; Li, Z.; Zhou, Y.; Xing, X.; Wang, Z.; Yang, Q. First principles investigation on interface properties and formation mechanism of γ-Fe/CeO2 heterogeneous nucleation interface. *J. Alloys Compd.* **2020**, *831*, 154867. [CrossRef]
3. Wang, J.; Enomoto, M.; Shang, C. First-principles study on the interfacial segregation at coherent Cu precipitate/Fe matrix interface. *Scr. Mater.* **2020**, *185*, 42–46. [CrossRef]
4. Sandelin, R.W. *Galvanizing Characteristics of Different Types of Steel*; American Hot Dip Galvanizers Association: Centennial, CO, USA, 1940.
5. Kozdras, M.; Niessen, P. Silicon-induced destabilization of galvanized coatings in the sandelin peak region. *Metallography* **1989**, *22*, 253–267. [CrossRef]
6. Bondareva, O.; Melnikov, A. Effect of the silicon content in steel on the hot-dip zinc coating microstructure formation. *IOP Conf. Ser. Mater. Sci. Eng.* **2016**, *156*, 012015. [CrossRef]
7. Wen, L.; Ai, L.; Hong, L.; Zhou, Y.; Zhu, G.; Sun, C. Diffusion Behavior of Carbon and Silicon in the Process of Preparing Silicon Steel Using Solid-State Decarburization. *Processes* **2023**, *11*, 3176. [CrossRef]
8. So, S.-M.; Grandhi, S.; Kwon, E.-P.; Oh, M.-S. Effects of Si Addition on Interfacial Microstructure and Corrosion Resistance of Hot-Dip Zn–Al–Mg–Si Alloy-Coated Steel. *Crystals* **2024**, *14*, 294. [CrossRef]
9. Sun, Y.; Wang, Z.; Du, M.; Du, Y.; Zhang, W. First-principles study on Si atom diffusion behavior in Ni-based superalloys. *Materials* **2023**, *16*, 5989. [CrossRef]
10. Wang, Q.; Zhao, Z.; Bai, P.; Du, W.; Liao, H.; Li, Y.; Liang, M.; Huo, P.; Zhang, L.; Tie, D. Effects of alloying elements X (Cr, Mn, Mo, Ni, Si) on the interface stability of TiC (001)/γ-Fe (001) in TiC/316L stainless steel composite formed by selective laser melting: First principles and experiments. *Adv. Compos. Hybrid Mater.* **2021**, *4*, 195–204. [CrossRef]
11. Peng, C.; Zeng, L.; Huang, F.; Zhong, M.; Liang, S.; Ran, X.; Zhou, L. Effects of alloying elements on mechanical and electronic properties of Cu by first-principles calculations. *IOP Conf. Ser. Mater. Sci. Eng.* **2020**, *772*, 012064. [CrossRef]
12. Paez-Ornelas, J.; Fernández-Escamilla, H.; Takeuchi, N.; Guerrero-Sánchez, J. Adsorption and diffusion mechanisms of silver ad-atoms on Ag and Cu (110) surfaces: A first principles study. *Mater. Today Commun.* **2020**, *25*, 101461. [CrossRef]
13. Chen, W.; La, P.; Yin, R.; Wan, L.; Du, Y.; Zheng, Y. Ab initio study of the energetics, electronic properties, and chlorine migration behavior of b2-feal (110) surface by microalloying. *Crystals* **2024**, *15*, 46. [CrossRef]
14. Lee, S.-J.; Lee, Y.-K.; Soon, A. The austenite/ε martensite interface: A first-principles investigation of the fcc Fe (1 1 1)/hcp Fe (0 0 0 1) system. *Appl. Surf. Sci.* **2012**, *258*, 9977–9981. [CrossRef]
15. Ren, J.; Hou, P.; Gao, Q.; Wang, Q.; Bai, Y.; Li, J.; Xue, H.; Lu, X.; Tang, F. A comparative study of the interfacial bonding properties and thermodynamic properties of bcc-Fe/MeAl (Me= Ni, Ti, Fe) interfaces based on first-principles methods. *J. Phys. Chem. Solids* **2025**, *202*, 112679. [CrossRef]
16. Gao, Q.; Qiao, G.; Wang, W.; Ge, Y.; Ren, J.; Li, W.; Yang, P.; Lu, X.; Qiao, J. The first-principles study of interfacial bonding strength and segregation behavior of alloyed elements at the η (MgZn 2)/Al interface. *Phys. Chem. Chem. Phys.* **2024**, *26*, 17240–17254. [CrossRef] [PubMed]
17. Kabi, O.; Abu-Jafar, M.S.; Farout, M.; Mousa, A.A.; Bouhemadou, A.; Erum, N.; Azar, S.M.; Bassalat, A.; Abualrob, H.; Thabaineh, A.Y. Ab initio investigation of the structural, elastic, dynamic, electronic, and magnetic properties of cubic perovskite CeCrO3. *ACS Omega* **2024**, *9*, 11820–11828. [CrossRef]
18. Abdulhussein, H.A.; Hossain, M.A.; Hosen, A.; Dahliah, D.; Abu-Jafar, M.S.; Harbi, A.; Pingak, R.K.; Moutaabbid, M.; Ovi, I.A.; Islam, M.R. A comprehensive analysis of the structural, phonon, electronic, mechanical, optical, and thermophysical properties of cubic Ca3SbX3 (X= Cl, Br): DFT-GGA and mBJ studies. *Mater. Sci. Semicond. Process.* **2025**, *187*, 109133. [CrossRef]
19. Sun, B.; Ding, F.; Qiu, B.; Guo, J.; Cao, T. First principles investigation of in-situ NiAl (110)/Ag (111) and NiAl (110)/MoO3 (010) heterogeneous interfaces behavior in composite coatings. *Surf. Interfaces* **2024**, *48*, 104328. [CrossRef]
20. Wang, H.; Gao, X.; Xing, L.; Tan, H.; Lin, H.; Gao, S. Segregation mechanism of alloying elements at the fcc-Fe/bcc-Fe interface and its effects on carbon diffusion across the boundary. *J. Phys. Chem. Solids* **2023**, *183*, 111657. [CrossRef]
21. Yuan, X.; Xiao, Y.; Wang, G.; Zhang, L. TiN inducing ferrite nucleation based on the bcc-Fe/TiN interfaces formation at atomic scale by first-principles calculation. *Comput. Mater. Sci.* **2021**, *197*, 110570. [CrossRef]
22. Zhang, G.; Zhang, Y.; Xu, H.; Yu, H. Strong bonding effect and Zn segregation et Al/Fe bimetallic composite interface: A first-principles study. *J. Mater. Res.* **2023**, *38*, 3078–3088. [CrossRef]
23. Zhang, L.; Li, Y.; Zhou, R.; Wang, X.; Wang, Q.; Xie, L.; Li, Z.; Xu, B. First-principles study of the effect of sn content on the structural, elastic, and electronic properties of Cu–Sn alloys. *Crystals* **2023**, *13*, 1532. [CrossRef]
24. Liu, B.; Yang, J. Mg on adhesion of Al (111)/3C-SiC (111) interfaces from first principles study. *J. Alloys Compd.* **2019**, *791*, 530–539. [CrossRef]

25. Feng, Y.; Chen, X.; Hao, Y.; Chen, B. Characterization and energy calculation of the S/Al interface of Al–Cu–Mg alloys: Experimental and first-principles calculations. *Vacuum* **2022**, *202*, 111131. [CrossRef]
26. Han, Y.; Dai, Y.; Wang, J.; Shu, D.; Sun, B. First-principles calculations on Al/AlB2 interfaces. *Appl. Surf. Sci.* **2011**, *257*, 7831–7836. [CrossRef]
27. Wang, S.; Ye, H. Theoretical studies of solid–solid interfaces. *Curr. Opin. Solid State Mater. Sci.* **2006**, *10*, 26–32. [CrossRef]
28. Lu, S.; Hu, Q.-M.; Punkkinen, M.P.; Johansson, B.; Vitos, L. First-principles study of fcc-Ag/bcc-Fe interfaces. *Phys. Rev. B Condens. Matter Mater. Phys.* **2013**, *87*, 224104. [CrossRef]
29. Xie, Y.; Wang, D.; Yin, Y.; Li, J.; Li, W.; Liu, Z.; Ji, X.; Wan, Q.; Shen, X.; Zhou, J. Investigation on the interface properties of Be-Al alloys via first-principles calculation. *Mater. Today Commun.* **2024**, *40*, 109972. [CrossRef]
30. Zhao, X.; Zhuo, Y.; Liu, S.; Zhou, Y.; Zhao, C.; Wang, C.; Yang, Q. Investigation on WC/TiC interface relationship in wear-resistant coating by first-principles. *Surf. Coat. Technol.* **2016**, *305*, 200–207. [CrossRef]
31. Lu, S.S.; Chang, Y.L. The accurate evaluation of lattice spacings from back-reflection powder photographs. *Proc. Phys. Soc.* **1941**, *53*, 517. [CrossRef]
32. Jette, E.R.; Foote, F. Precision determination of lattice constants. *J. Chem. Phys.* **1935**, *3*, 605–616. [CrossRef]
33. Wedig, U.; Nuss, H.; Nuss, J.; Jansen, M.; Andrae, D.; Paulus, B.; Kirfel, A.; Weyrich, W. Electronic origin of the structural anomalies of zinc and cadmium. *Z. Anorg. Allg. Chem.* **2013**, *639*, 2036–2046. [CrossRef]

Disclaimer/Publisher's Note: The statements, opinions and data contained in all publications are solely those of the individual author(s) and contributor(s) and not of MDPI and/or the editor(s). MDPI and/or the editor(s) disclaim responsibility for any injury to people or property resulting from any ideas, methods, instructions or products referred to in the content.